Principal Facts and an Approach to Collecting Gravity Data Using Near-Real-time Observations in the Vicinity of Barstow, California

By G. Phelps, C. Cronkite-Ratcliff, and L. Klofas

Open-File Report 2013–1264

U.S. Department of the Interior
U.S. Geological Survey

U.S. Department of the Interior
SALLY JEWELL, Secretary

U.S. Geological Survey
Suzette M. Kimball, Acting Director

U.S. Geological Survey, Reston, Virginia: 2013

For product and ordering information:
World Wide Web: http://www.usgs.gov/pubprod
Telephone: 1-888-ASK-USGS

For more information on the USGS—the Federal source for science about the Earth,
its natural and living resources, natural hazards, and the environment:
World Wide Web: http://www.usgs.gov
Telephone: 1-888-ASK-USGS

Suggested citation:
Phelps, G., Cronkite-Ratcliff, C., and Klofas, L., 2013, Principal facts and an approach to collecting gravity data using near real-time observations in the vicinity of Barstow, California: U.S. Geological Survey Open-File Report 2013–1264, 24 p., http://pubs.usgs.gov/of/2013/1264/.

Contents

Figures

Principal Facts and an Approach to Collecting Gravity Data Using Near-real-time Observations in the Vicinity of Barstow, California

By G. Phelps, C. Cronkite-Ratcliff, and L. Klofas

Abstract

A gravity survey was done in the vicinity of Barstow, California, in which data were processed and analyzed in the field. The purpose of the data collection was to investigate possible changes in gravity across mapped Quaternary faults and to improve regional gravity coverage, adding to the existing national gravity database. Data were collected, processed, analyzed, and interpreted in the field in order to make decisions about where to collect data for the remainder of the survey. Geological targets in the Barstow area included the Cady Fault, the Manix Fault, and the Yermo Hills. Upon interpreting initial results, additional data were collected to more completely define the fault targets, rather than collecting data to improve the regional gravity coverage in an adjacent area. Both the Manix and Cady Faults showed gravitational expression of the subsurface in the form of steep gravitational gradients that we interpret to represent down-dropped blocks. The gravitational expression of the Cady Fault is on trend with the linear projection of the mapped fault, and the gravitational expression of the Manix Fault is north of the current northernmost mapped strand of the fault. The relative gravitational low over the Yermo Hills was confirmed and better constrained, indicating a significant thickness of sediments at the junction of the Calico, Manix, and Tin Can Alley Faults.

Acknowledgments

This work was made possible by the National Geologic Mapping Act of 1992, and D.M. Miller provided project overview, guidance, and discussions. The manuscript was significantly improved through discussions with D. Scheirer and R. Saltus, as well as their careful reviews. The authors would like to extend their appreciation to all who made this work possible.

Introduction

The U.S. Geological Survey completed a gravity survey with the intent of collecting, processing, analyzing, and interpreting field data in as near real-time as possible. This approach allows for additions and modifications to the original survey plan during the course of the survey, based on interpretive results derived from field data. Such modifications to the survey offer the possibility of significantly increasing scientific productivity because new hypotheses can be generated and tested in a single field session.

We conducted two surveys in the Mojave Desert, one in 2010 and one in the 2011. The surveys were designed to investigate possible gravitational expression across several predominantly left-slip Quaternary faults and their proposed extension where buried by thick sediment cover, and to improve the regional gravity data coverage. The data were collected across a 60-km-wide region from approximately 23 km east of Barstow, Calif., on the west to Ludlow, Calif., on the east (fig. 1). Data from tightly spaced gravity stations (200–300 m spacing) were collected along roads that cross Quaternary faults (fig. 2). Data collected along such lines, typically oriented perpendicular to the strike of a fault, can be used to model subsurface density changes that might result from an offset of a dense rock unit across a fault, providing estimates of the magnitude of the offset. To increase the sample density of the regional gravity dataset in areas of sparse data coverage, data from additional stations (spaced from 500 m to 1 km) were also collected. The first survey (2010) was intended primarily to increase the regional gravity-data coverage, and the second survey (2011) focused primarily on gravity changes across specific faults. The second gravity survey (2011) also investigated the application of near-real-time collection, processing, analyzing, and interpretation of gravity data.

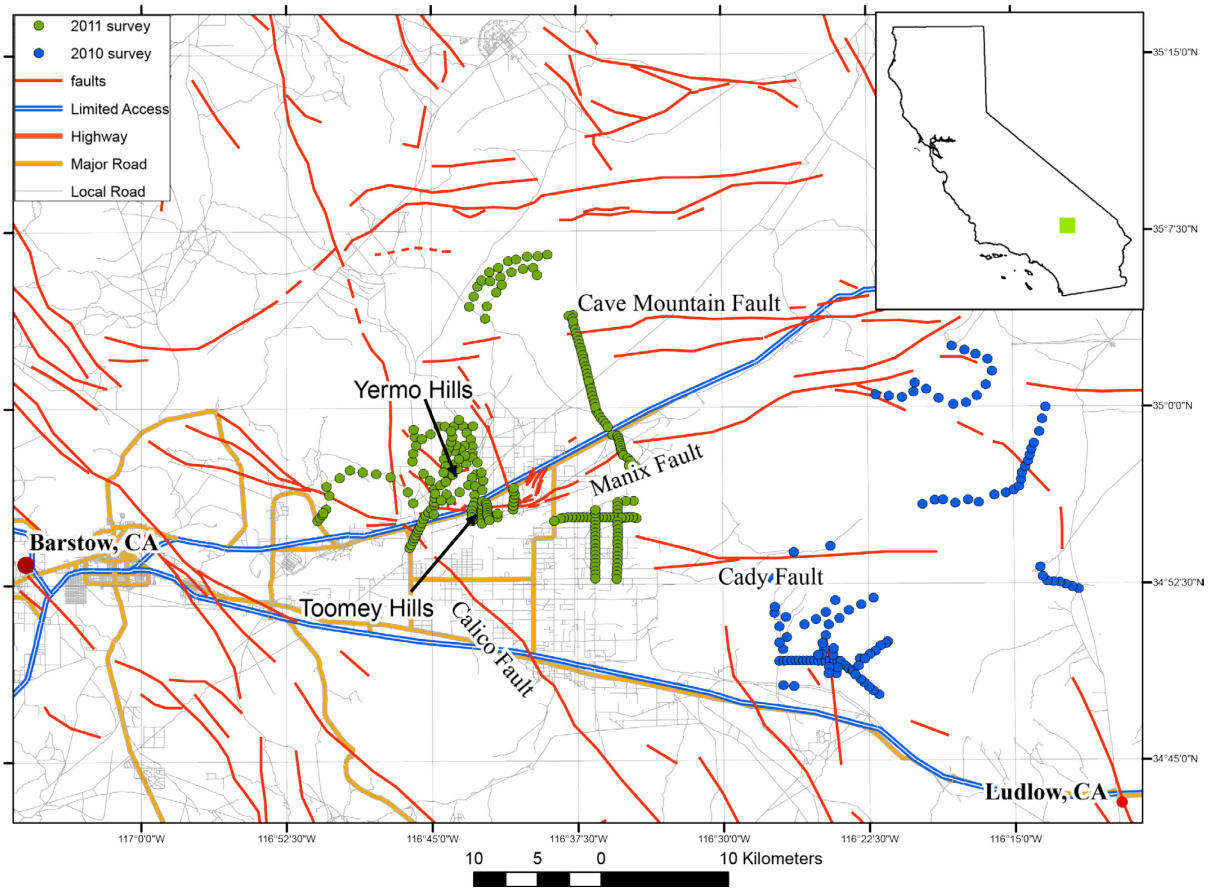

Figure 1. Location of newly collected gravity data, Barstow, California. Base road map from ESRI (TM) digital map of the world. Map projection UTM zone 11 NAD83.

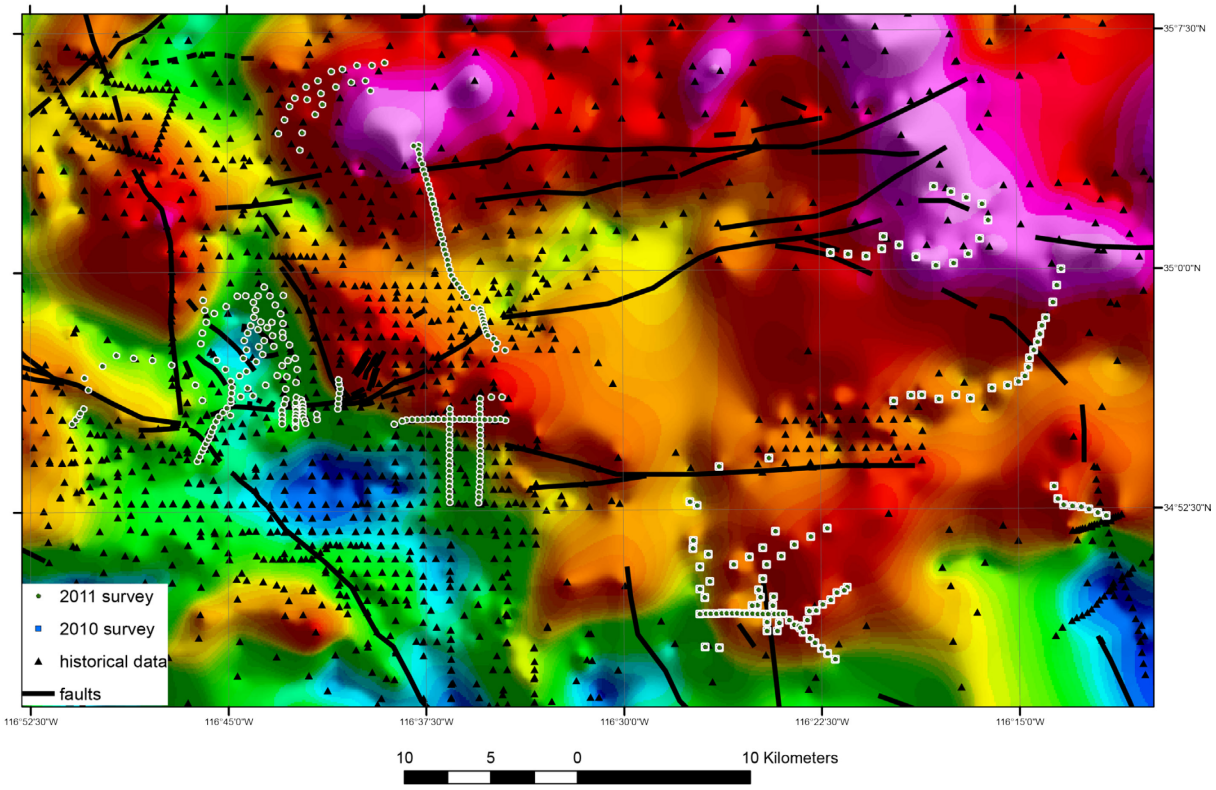

Figure 2. Isostatic residual gravity surface interpolated from the recently collected and historical data, Barstow, California. Map projection UTM zone 11 NAD83. Cool colors indicate lower, and warm colors indicate higher, isostatic residual gravity.

Recent investigations mapping Quaternary geology in the eastern Mojave Desert have highlighted newly discovered Quaternary faults (Miller and others, 2007), many of which strike north or east, directions not predicted by tectonic models proposed for the region (Garfunkel, 1974; Dokka and Travis, 1990; Ron and others, 2001). Discovery of these faults indicates that existing tectonic models do not fully explain the observed structural complexity. Mapping of these faults is on-going, and interpretation of the surface extent of fault traces is complicated by limited exposure, erosion of existing exposures, and complex surface expression. Tools that trace faults beneath Quaternary cover are needed to map the extent and behavior of the faults where they are not exposed.

Measuring the gravitational field at the Earth's surface is often an effective tool for constraining paths of faults in the subsurface. Faults commonly juxtapose rocks of differing density, which causes measurable changes to the local gravitational field across the contact between the two rocks, provided the contact is vertical to subvertical (horizontal changes in density cause a datum shift only in the gravitational anomaly). Many of the recently mapped Quaternary faults in the study region are interpreted to be strike-slip and, therefore, meet the criterion of a vertical to subvertical contact. If these faults juxtapose rocks of differing density, then the contact can be modeled by using gravity data. Such models can be helpful in regions of poor exposure, or where the surface material is not cohesive enough to preserve fault scarps for more than a few years.

Existing gravity measurements in the greater Barstow, Calif., area are sparse and unevenly distributed across the landscape (fig. 2). Because the resolution of a gravity model is limited by the spacing of the gravity measurements, regions of sparse data coverage are also regions of comparatively low resolution. Many areas in this region have spacings of about 3 km, some as close as 1 km and others as sparse as 6 km. Such spacings are not dense enough to resolve structures that are approximately from 2 to 10 km long. The resolution can be enhanced by collecting additional data in areas of sparse data coverage.

We collected 359 new gravity stations (measurements of the Earth's gravitational field at a given location) with spacings between 200 m and 1 km, locating the spatially dense stations in lines approximately perpendicular to mapped or suspected Quaternary faults (fig. 2). The data were processed, added to an existing gravity dataset previously compiled from several sources (Snyder and others, 1982; Biehler and others, 1988; Langenheim and others, 2009; Pan-American Center for Earth and Environmental Studies, 2010; C.W. Roberts, United States Geological Survey, unpub. data, 2008), and used to create cross-sectional models that highlight structural offsets in the subsurface that may be indicative of faulting.

For the 2011 field season, we used hand-held devices that delivered high-resolution satellite imagery, GPS location data, and spreadsheet capability as well as laptop computers capable of complete gravity data reduction processing and gravity modeling. We collected, processed, and interpreted the gravity data and constructed several simple geologic cross-sections across mapped and potentially buried Quaternary fault strands, based on the newly acquired gravity data. The modeled cross-sections are an example of developing hypotheses, which were subsequently tested by further gravity data collection and modeling.

Working toward near-real-time data processing and analysis is significant because, when achieved, it will allow scientific investigators to model subsurface geology "on-the-fly," and generate hypotheses that can be tested immediately, rather than requiring investigators to process and generate models in the office days to weeks later and wait for a subsequent field session to test these models.

Method

The data collection and processing method include upgraded technology used in field data collection, detailed assessments of uncertainty introduced by elevation and instrument drift, and modeling specifications and modeling uncertainty envelopes.

Survey

Data were collected to improve the regional gravity data coverage (fig. 2; appendix I) and to investigate local faulting. Densely sampled (200–300 m) survey lines were established perpendicular to Quaternary faults in order to characterize gravity anomalies that might exist if motion on a fault juxtaposed rocks or soil of differing densities (figs. 3 and 4). The 2010 survey was done using traditional methods of field data collection followed by post-fieldwork data processing in the office. The 2011 survey incorporated technological advances that have become available over during the past ten years into the field data workflow, so that processing and modeling was ongoing during field data collection.

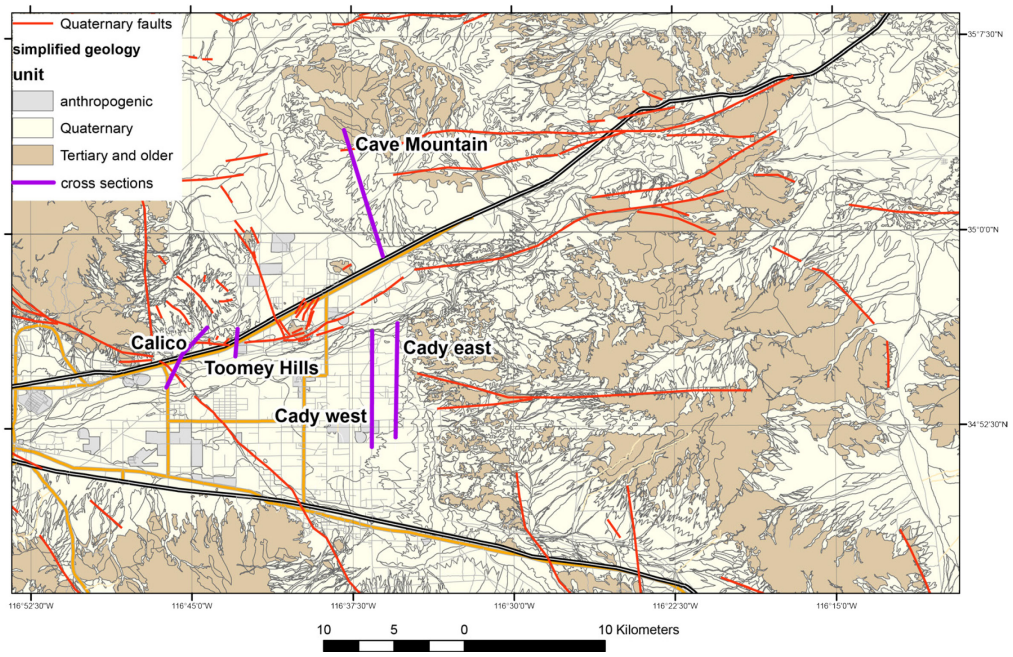

Figure 3. Location of cross-sections (purple lines), Barstow, California. Black triangles show the location of historical gravity stations. See figure 1 for explanation of road network base map. Simplified geology from Phelps and others (2011). Map projection UTM zone 11 NAD83.

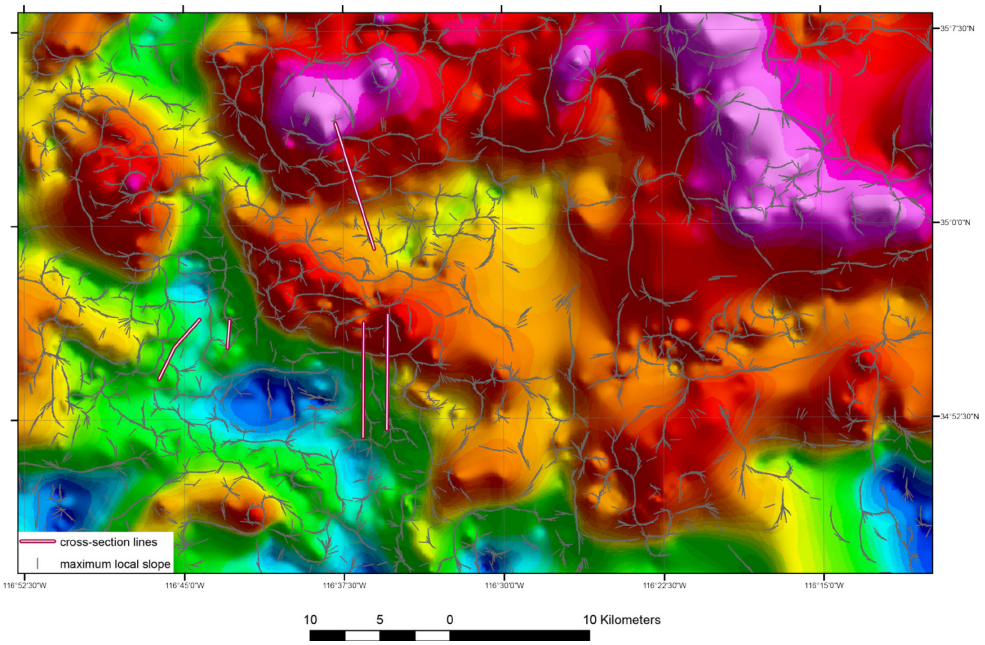

Figure 4. Location of points of maximum local slope, displayed as short line segments aligned parallel to surface contours, Barstow, California. White lines are cross-section lines, thick black lines are Quaternary faults, and the color-contoured surface is the interpolated isostatic residual gravity. Map projection UTM zone 11 NAD83.

Technological Advances

Several technological improvements were implemented in the 2011 survey, including modified gravimeter with an output in mGal (or easily converted to mGal), a high-precision GPS device capable of delivering post-processed positions corrected within 24 hours, geophysical software for data reduction and analysis, and an iPad tablet (used for navigation) with 3G communication, capable of displaying satellite imagery served from Google Maps, with software capable of uploading and downloading GIS files in a common data format (ESRI shape files). Most of these advances have been available for several years, but they had not been incorporated into the gravity field data collection workflow. The data were collected, processed, analyzed, and interpreted in the field. Preliminary results from the field interpretation were used to make decisions regarding data collection for the remainder of the survey.

Gravity station values were collected by using a LaCoste-Romberg gravimeter with modified electronics (an "Aliod" gravimeter) that perform the instrument and Earth-tide corrections internally, so that the gravimeter measurements are output in units of mGal, the standard unit for gravitational measurements. A hand-held Palm computer with an internal GPS was attached to the gravimeter and used to determine an approximate location sufficient to calculate the tidal correction. Because LaCoste-Romberg gravimeters measure the change in the gravitational field, not the absolute value, measurements must be tied to a base station where the value of the gravitational field (the "observed gravity") is known. The observed gravity values at field stations were calculated from the value of the observed gravity at the base station and the mGal offset reported by the gravimeter.

The instrument was checked for consistent behavior by measuring at the base station at the beginning and end of each survey day. Additionally, repeat measurements were made at previously occupied gravity stations periodically throughout the survey. These repeat measurements were used to assess the precision of the measurements, as described below. Instrument-drift correction, a correction typically applied to gravity measurements, was not applied in this survey for reasons discussed in the following section.

Locations were measured using a Trimble GeoXH Global Positioning System (GPS) that records dual-frequency carrier-phase data. This system uses H-star technology (Trimble Navigation Limited, 2005), with reported positional accuracies that are often less than 15 cm in the horizontal direction and 20 cm in the vertical direction after post-processed differential corrections are applied. Positional information was collected simultaneously with the gravity-data collection. Post-processing, where GPS locations are corrected by using time-varying factors established at known GPS reference stations in the region, was performed each night to achieve the highest accuracy position. Post-processing was performed with Trimble Pathfinder Office™ software. The base-station files were available on the Internet within 24-48 hours of collecting the data; therefore, accurate positions for gravity stations were received 1–2 days after the data were collected.

For the 2011 survey, the reduction process was performed as soon as the post-processed GPS locations were available, typically within 24 hours, and always within 48 hours, of collecting the data. During the first few days of the 2011 survey, gravity data were collected along three profile lines, each of which was designed to investigate any gravitational expression across the extension of mapped Quaternary faults beneath Quaternary alluvial cover. A key decision that needed to be made during the survey was whether to collect additional data along parallel transects to better constrain the faults in the subsurface along-strike, or whether the remainder of the survey should be spent collecting data in another region. To address this

question, the reduced gravity was modeled along three profiles collected perpendicular to the linear projections of three faults: the Manix Fault south of the Alvord Mountains, the Cady Fault, and the westernmost strand of the Manix Fault mapped along the base of the Toomey Hills. GMSYS 2D (Geosoft, Inc.) software was used for cross-section modeling. The modeled profiles indicated that the Cady Fault definitely displaces bedrock beneath the alluvial cover, that the Manix Fault south of the Alvord Mountains seems to displace bedrock beneath alluvial cover just north of where it is mapped, and that the westernmost strand of the Manix Fault along the base of the Toomey Hills may displace bedrock (note that in this context "bedrock" refers to any lithified rock that forms a basin and is distinct from the unconsolidated material filling the basin). Each of these results warranted closer investigation of each fault, and the remainder of the survey was spent collecting data on transects parallel to the initial ones.

Fieldwork was greatly improved by using an iPad. Running the free app IGIS and using the device's internal GPS, the approximate location of the vehicle was tracked instantly on high-resolution satellite-based imagery served from Google. Survey lines and planned station locations were uploaded from the field computer to the tablet the night before each survey day to help guide data collection. The approximate locations of measurement stations (using the tablet's internal GPS) were recorded and stored in IGIS to assist with navigation and to make an overview of the survey continually available. The recently acquired high-resolution satellite imagery was helpful in navigating back roads and jeep trails that do not appear or are incorrectly marked on older maps, such as topographic maps, that are commonly used during fieldwork. Both IGIS and spreadsheet apps were used to record data collected in the field. Data were downloaded and backed up each night on multiple devices (laptop computers and portable disk drives) to protect the data in the event of catastrophic equipment failure.

Assessing Instrument Drift

Gravimeter measurements are known to drift over time (Dobrin and Savit, 1988; Lowrie, 1997). When all other known influential factors have been taken into account, repeat measurements at the same location will vary in a temporally correlated way during the course of a day or several days, sometimes gradually increasing or decreasing monotonically, sometimes increasing and decreasing in a quasi-periodic fashion. This unpredictable, nonlinear drift is usually attributed to small changes in temperature and elasticity of the instrument's internal spring (Telford and others, 1990; Lowrie, 1997).

Any correction for instrument drift during regional surveys (where repeat station measurements are limited) must proceed by demonstrating or assuming: (1) that the magnitude of the random error is significantly less than the magnitude of the instrument drift, (2) that the function representing the instrument drift can be well approximated, and (3) that sufficient repeat data are collected to model this function within acceptable error limits.

For the 2010 and 2011 surveys, the relative-gravity measurements made at the base station each morning were set to the base station observed-gravity measurement, so that all of the gravity station readings throughout the day were measured relative to the morning base-station reading. Instrument drift greater than one day is, therefore, not a factor in these measurements.

Correction for instrument drift during a survey day has been accomplished in the past by measuring at repeat stations at short (approximately two hour) intervals, during which time the drift is assumed to be linear (Nettleton, 1971; Telford and others, 1990). However, for regional surveys that typically involve traversing long distances (tens of kilometers or more) in a single day, it can be impractical to return to a base station every two hours. In this case instrument drift

must be assessed by evaluating any repeat measurements that are taken within a given day. Although there are typically not enough repeat measurements to model the drift function and compensate for it, the recorded changes can be assessed and factored into the error budget. If the introduced error is acceptably low, then any error due to instrument drift can be reported as part of the total error budget. This was the method that was used in this survey.

Repeat measurements were made throughout the survey. We then calculated the change for each temporally adjacent pair of readings at the same location (consecutive readings) and the time between readings. These data were then plotted to determine plausible functions for instrument drift.

The change in gravity for each day was plotted for the entire 2011 survey (fig. 5). The initial value for the change in gravity was set to zero, and, if the time difference between the two measurements was greater than two hours, the initial and final values were connected by a red line. For pairs less than two hours apart, the red line was not shown because it would be nearly vertical. Figure 5 shows whether repeat stations taken in overlapping time intervals have the same direction and magnitude of apparent instrument drift. Note that sometimes temporally overlapping repeat stations show a similar increase or decrease, but that at other times the data contradict the notion of a single direction of change during the time interval.

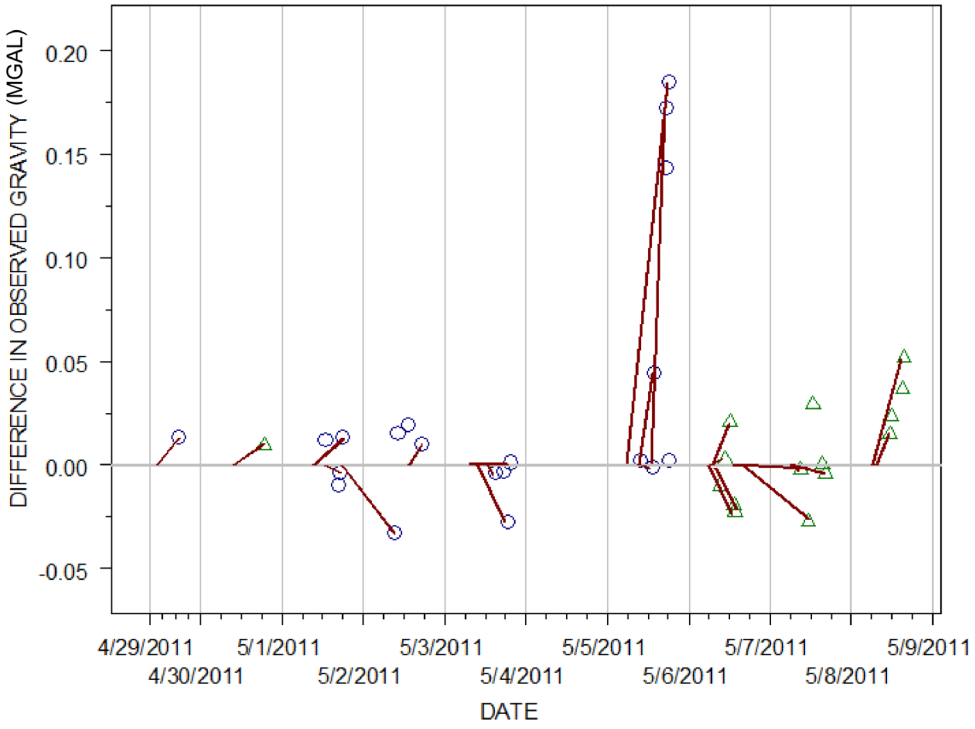

Figure 5. Difference in observed gravity between pairs of consecutive repeat measurements collected during the 2011 survey. Initial reading is set to zero, and the final measurement is shown as a blue circle (G8-N) or a green triangle (G-425). A red line connects the initial and final readings of each measurement pair (for measurement pairs taken more than two hours apart). The slope of the red line shows the apparent rate of change occurring between the initial and final measurements. Note that no consistent rate of change across any given time is observed.

The rate of change in gravity (in mGal per hour) for the same repeat pairs was plotted against time over the entire survey for each gravimeter (fig. 6A, B). This graph is designed to address the assumption that instrument drift can be modeled as a linear function.

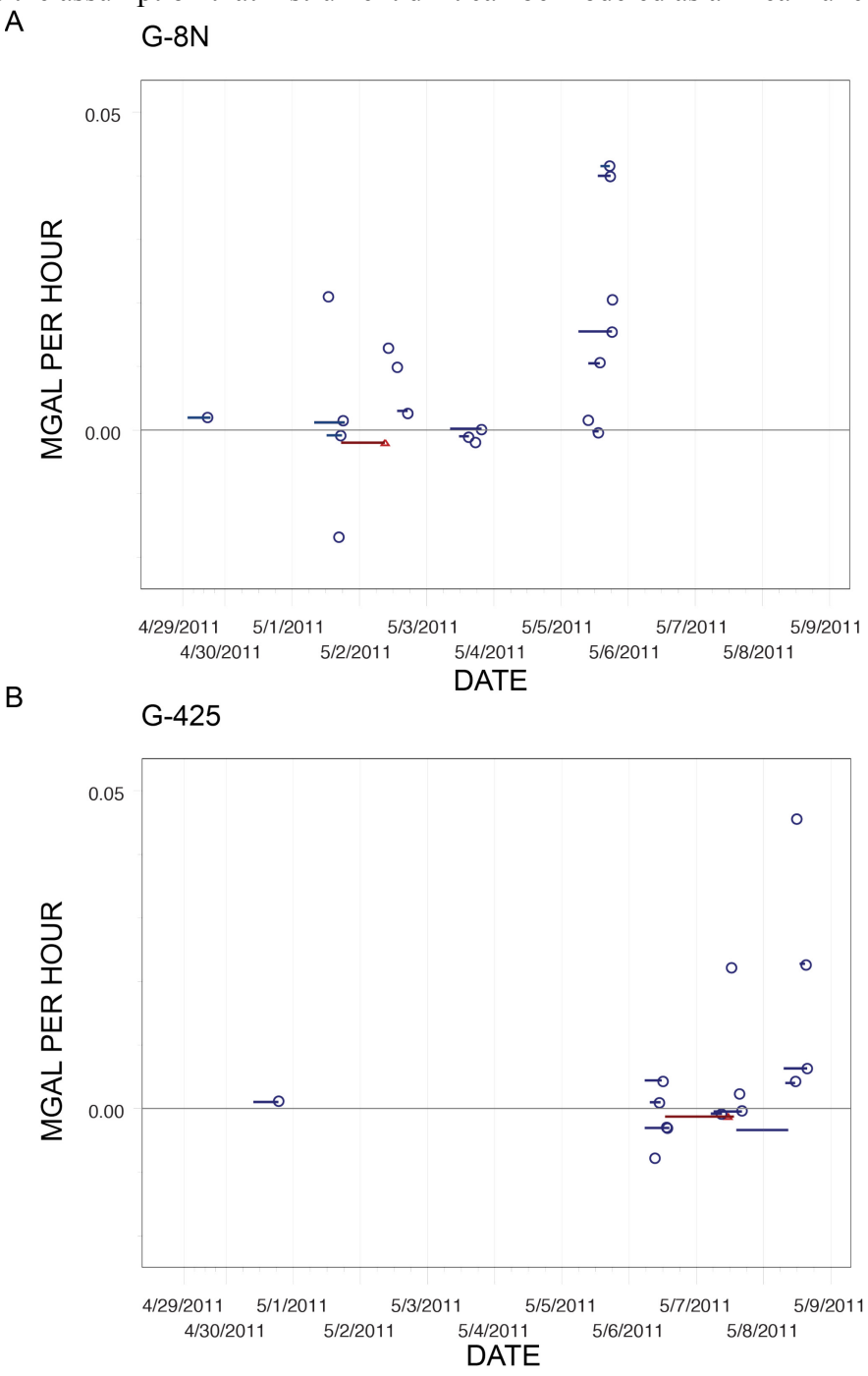

Figure 6. Apparent rate of change of instrument drift as measured by consecutive repeat measurements collected during the 2011 survey. Blue circles show data collected during the day, red triangles show data collected overnight. Horizontal lines mark time between the initial and final measurement for each data pair. *A*, Gravimeter G-8N. *B*, Gravimeter G-425.

A linear-drift function would have a constant rate of change, so that multiple measurement pairs would plot along the same horizontal line if the gravimeter exhibited a consistent linear drift during a given time interval. However, neither gravimeter shows consistent linear-drift behavior. Pairs of measurements spanning overlapping time intervals can show contradictory behavior (see, for example, the behavior of G8-N on May 1), indicating that changes due to instrument drift are not linear during that time span. Shorter time-span repeat readings are often variable in their linear rate of change, likely because random measurement error has a larger effect on the calculation of slope at short time intervals. Rates of change for longer time spans are less than 0.005 mGal per hour. This is the behavior expected from measurements in which the component of random error was contributing significantly to the differences observed for repeat measurements; the apparent rate of change would shrink with longer time spans because the denominator (time) is increasing and the numerator is remaining fixed by the range of the random error. Figure 7 shows the rate of change as a factor of time between readings. Higher rates of change can be seen for shorter time intervals and for repeat measurements made during the work day. As the time interval increases to about 12 hours, the rate tends to zero (fig. 7).

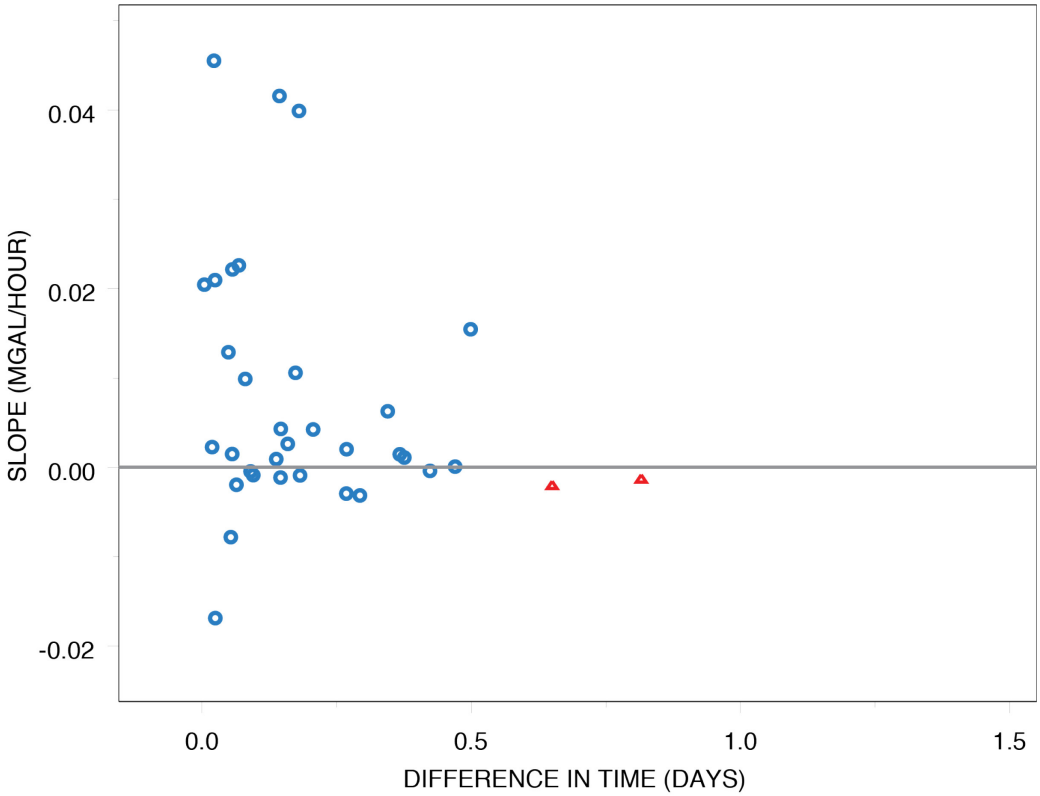

Figure 7. Apparent rate of change due to instrument drift plotted against the difference in time between the initial and final reading for each consecutive repeat measurement collected during the 2011 survey. Blue circles are data recorded during the day, red triangles are data recorded overnight.

The overall conclusions reached from this analysis are: (1) that the error introduced by daily instrument drift in this survey is less than that of other sources of random error, (2) that the drift function is probably nonlinear, and (3) that the function cannot be adequately characterized

during the course of a typical survey, even when an effort is made to collect multiple repeat readings and even during time intervals as short as two to three hours. Any existing instrument drift must be treated as part of the random error of the instrument in this survey.

If we were to ignore these observations and attempt to model daily instrument drift by applying a linear function to the first and last base reading of the day, there is a risk of increasing both the error for many observations and the RMS error. Consider a fictitious example (based on actual observations of the behavior of the G8-N meter) where the drift curve is somehow known to exhibit a hockey-stick pattern during a four-hour period. During this four-hour period, six measurements are taken per hour. The meter does not drift appreciably for almost three hours, then suddenly drifts approximately linearly for the remainder of the time period, up to a net increase of 0.03 mGal (fig. 8, circles). A perfect model for drift would follow this hockey-stick curve. However, the true instrument drift is not known during typical regional surveys. If an attempt is made to model the instrument drift as a linear function based on the first and last readings of this time period, the result would be an overcorrection of the data. Figure 8 shows this overcorrection, the result of applying a linear model to the true hockey-stick instrument drift (fig. 8, triangles). The application of a linear model to this case increases the error for most of the measurements and increases the total RMS error slightly (by approximately 3 μGal). A few data points towards the end of the time period are improved at the expense of most of the data.

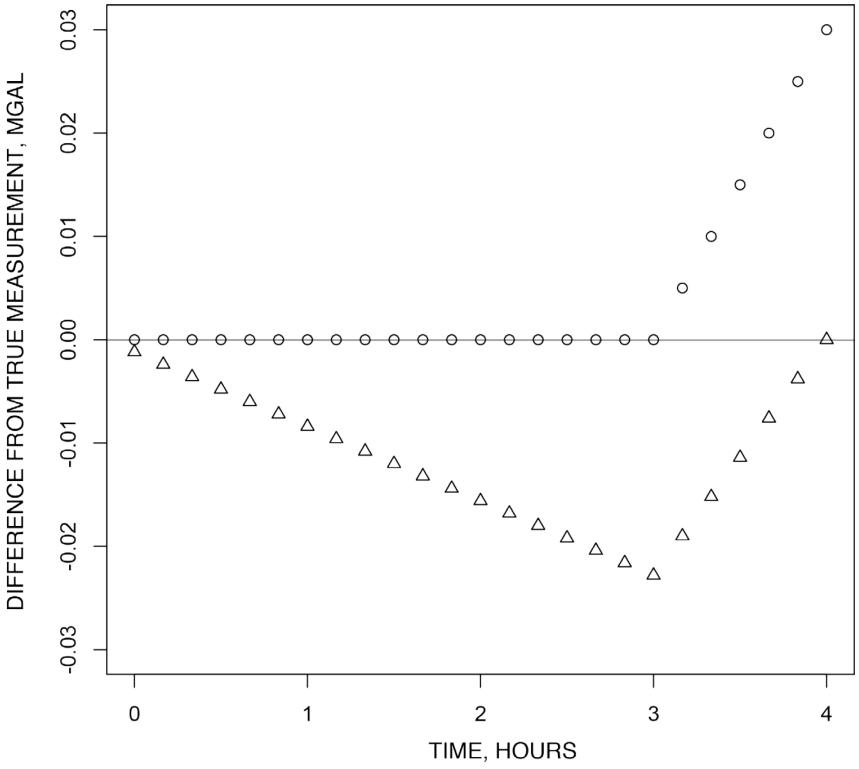

Figure 8. Example of applying an incorrect model of instrument drift. Circles indicate true (typically unknown) instrument drift, which shows the deviation from the true measurement. Triangles show the deviation from the true measurement after subtracting from the data a linear model of instrument drift that is based on the first and last measurement.

The repeat stations taken during the 2011 survey allow for the estimation of measurement error and any additional instrument drift. The standard deviation of the measurement differences for repeat stations is approximately 0.05 mGal (fig. 9).

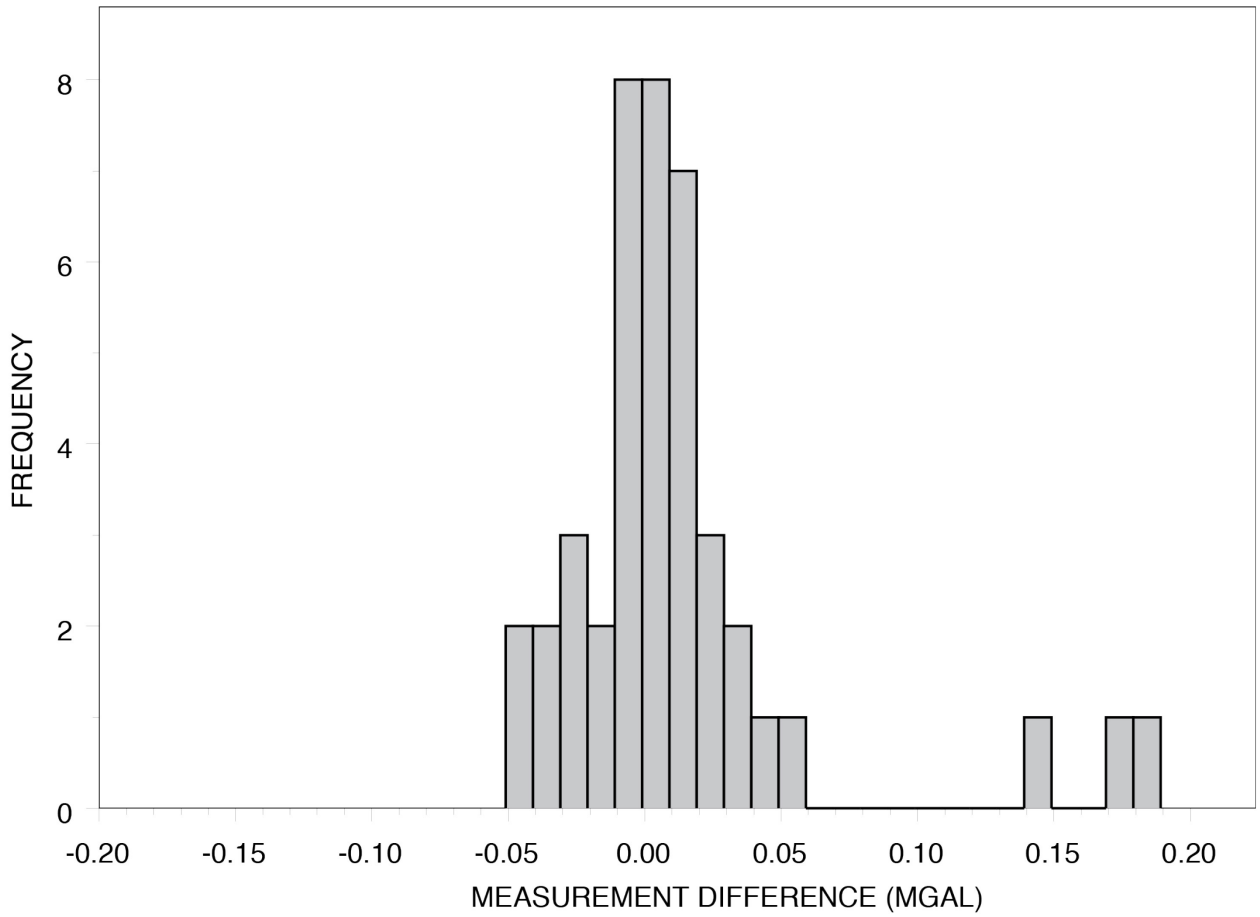

Figure 9. Histogram of the difference in repeat readings for consecutive measurement pairs collected during the 2011 survey.

Data Reduction

Gravity data were referenced to International Gravity Standardization Net 1971 (Morelli, 1974) by measuring at local base stations with known absolute gravity. The base station used for the 2010 survey is located at the Ludlow motel (Langenheim and others, 2009) and has a reported observed gravity value of 979,506.32±0.02 mGal. The base station used for the 2011 survey was PB1018 of Roberts and Jachens (1986), who list a value of 979,492.864 mGal for the observed gravity. An updated location of base station PB1018 was acquired using the Trimble GeoXH GPS system: easting 514500.7 m, northing 3865231.0 m, elevation 656.10 m, with horizontal coordinates given in UTM zone 11 NAD83, and vertical coordinates given in NAVD88.

Standard gravity-data corrections of latitude, free air, simple Bouger, curvature, terrain, and isostasy, as described by Blakely (1995), were applied to the observed gravity and calculated using the software Oasis Montaj (Geosoft, Inc., 2006). The latitude of the gravity measurements

is used to compensate for the elliptical shape of the Earth and its rotation. The free-air correction compensates for the reduction in gravity caused by increasing the distance from mean sea level. The simple Bouger correction compensates for the mass between the gravimeter and mean sea level, assuming no terrain variations, and the curvature correction compensates for planar geometry of the simple Bouger correction. The terrain correction compensates for the effect of nearby topography, and the isostatic correction is a long-wavelength correction that compensates for mass deficits due to the isostatic roots of mountain ranges. Historical gravity stations were also re-reduced using this process to ensure the same corrections were applied in the same way to all stations.

Each step of the data reduction process was performed in Oasis Montaj and stored in a spreadsheet, so that each step in the reduction process could be examined and checked. The latitude correction was performed using the 1980 International Gravity Formula (Geosoft, Inc., 2006; Li and Gotze, 2001). The free-air correction was performed by using a constant elevation multiplication factor of 0.308596 mGal/m (Geosoft, Inc., 2006). This approximation introduces a slight bias of up to approximately 0.1 mGal between the lower elevation values and the higher elevation values [for example, when compared with the formula proposed by Swick (1942)]. The approximation is sufficient for modeling described in this paper, particularly because data that are close geographically are also close in elevation and, therefore, have little bias relative to one another. The curvature correction was calculated using La Fehr's (1991) formula. The terrain correction was calculated by using a combination of four sloping prisms for elevations next to the station, Nagy's method (1966) for elevations within 8 grid cells of the station, and Kane's method (1962) for elevations farther than 8 grid cells from the station, as described by Geosoft, Inc. (2006). Terrain corrections were estimated by using the Oasis Montaj software, which is set up to perform the estimate in two steps. The first step calculates an outer terrain correction, which for this dataset was calculated by using distances greater than 1 km from each station. The second step calculates an inner terrain correction, which for this dataset was calculated from the station out to a distance of 1 km. The outer terrain correction was estimated by using a terrain model derived from the 90 m resolution SRTM data, available online from the Geosoft DAP server (a public data server), resampled to a 500 m grid spacing. The inner terrain correction was estimated by using a 10 m grid spacing, a bilinearly interpolated terrain model derived from the 30 m U.S. Geological Survey National Elevation Dataset (Gesch, 2007; Gesch and others, 2002). The terrain correction was performed radially to a distance of 167 km. The density value used for bedrock in the Bouger and terrain corrections was 2,670 kg/m^3.

The isostatic correction was calculated by using the method of Simpson and others (1986); it was calculated radially to a distance of 167 km, using 30 km crustal thickness at sea level, a moho density contrast of 3,500 kg/m^3, and a topographic density of 2,670 kg/m^3; beyond that distance values were obtained from maps by Karki and others (1961).

The elevation of each station used to calculate the terrain correction deserves special mention. Because the terrain correction is calculated by using a digital elevation model (DEM), problems can occur if the measured GPS elevation does not agree with the terrain model. For example, if a station is located in an area of flat terrain, the local terrain correction should be zero over the region of constant elevation. If, however, the GPS elevation does not match the terrain model at that particular station location, locally an artificial slope will be introduced into the terrain calculation. This slope is due solely to the disagreement between the terrain model and GPS. Because the terrain correction is an estimated correction based upon the terrain model, the elevation of the station used for the terrain calculation was that of the terrain model, not the more

precise elevation recorded by the GPS. The elevation at each station, therefore, was interpolated directly from the terrain model (DEM), and this elevation was used for the terrain correction (the measured GPS elevation was used for all other calculations). In this way a consistent terrain model is used for the terrain correction, and anomalies due to differences in GPS and terrain-model elevation are avoided.

Reconciling Elevation Differences

Newly collected gravity data were processed by using the most modern geoid available (geoid2009) and were reduced to the mean sea level datum NAVD88. The historical gravity data, originally processed by using elevation values from USGS topographic maps using NGVD29 datum and the Clarke 1866 spheroid, were converted to NAVD88 by using the VERTCON program of the National Geodetic Survey (National Geodetic Survey, 2003). Upon comparing the elevation of the historical gravity data to newly collected gravity data at common locales, a systematic offset of approximately 1 m was observed. In order to reduce artifacts caused by datum shifts between newly collected data and historical gravity data, the elevation of the historical gravity data was adjusted to that of the newly collected gravity data by the systematic offset. Adjusting the historical data, rather than the new data, was the best choice because the locational accuracy of the historical data is moderate at best. Horizontal location information is stored only to the nearest 18 m for the historical data, and the source of the elevation is not preserved (but probably derived largely from topographic maps).

Historical gravity data were adjusted by comparing station elevations of both gravity data sets to an unpublished LiDAR data set, collected in 2004 over the Yermo Hills and vicinity (the geoid used to reference the elevation in the LiDAR data set is listed as geoid03). Within the LiDAR data footprint there are 359 newly collected gravity stations and 173 historical gravity stations. The gravity-station elevations were extracted, and the difference with the LiDAR dataset was calculated. Both sets of differences were approximately Gaussian, with the medians separated by 1.11 m. Thus, 1.11 m was subtracted from the historical gravity data set to remove the apparent shift between the data sets. With the data on the same baseline, the historical data were then combined with the newly collected data, and the combined dataset was used for further analysis.

Error Analysis

Error introduced by a combination of instrument error and instrument drift is approximately 0.05 mGal (see previous section). The free-air and simple Bouger corrections both depend on the estimated elevation. Gravity decreases due to distance from the Earth's center at an approximate rate of 0.3 mGal/m (Lowrie, 1997) of elevation above sea level. The simple Bouger correction reduces this value by approximately one-third, so the combined decrease in gravity with elevation is approximately 0.2 mGal/m. The uncertainty in elevation, as recorded by the Trimble GPS devices, is typically less than 0.3 m, and therefore, the uncertainty introduced by uncertainty in station elevation is less than 0.06 mGal. The latitude, curvature, terrain, and isostatic corrections are derived from Earth models, which may introduce bias according to the veracity of each model, but should introduce minimal interstation error. Because both old and new data were processed by using the same procedure, any biases should be consistent, and the relative gravity change between stations should not change appreciably.

The error at a given station relative to neighboring stations should, therefore, be less than 0.11 mGal (0.06 mGal elevation + 0.05 mGal instrument drift), or about 0.1 mGal. Stations with

poor vertical GPS position, hence a greater error introduced through the free-air and simple Bouger corrections, have been noted by including the vertical accuracy term for each station in appendix I. Note that the error associated with the historical gravity stations will likely be larger owing to the greater uncertainty in elevation for stations collected pre-GPS.

Modeling

Traverses with close spacing (200–300 m) were done across several structures of interest, improving the local resolution of the interpolated isostatic gravity anomaly surface. These traverses were forward-modeled in cross-section to investigate causative geologic structures. Forward modeling consisted of digitizing simple rock bodies, assigning densities to the bodies, and moving nodes until the gravity profile was matched. A simple two-layer density model was assumed for each profile. The upper layer consists of a less-dense package of idealized alluvial deposits, representing unconsolidated Quaternary sediments and any partly consolidated Tertiary deposits of similar density that might be present in the subsurface. The lower layer consists of a denser layer of idealized basement rocks, which represents both crystalline rocks and any Tertiary rocks that may be present and are of similar density. The polygons digitized for the forward gravity model are internally homogeneous and are assigned a single density value.

Densities for basement rocks in the model were set to the accepted average density of the crystalline rocks of the upper crust, 2,670 kg/m^3, while densities for idealized alluvial deposits were set to 2,000 kg/m^3. The latter density value is taken from the median of 177 borehole gravity samplings in Quaternary alluvium, similar to that found in the study area (summarized in Phelps and others, 1999). The standard deviation of these samplings is 170 kg/m^3. Variability in the density values of the alluvium reflects its heterogeneous nature. Because of this variability, the density assigned to the sedimentary overburden in the cross-sectional models is both uncertain and lacks appropriate heterogeneity. Modeling the alluvium as less dense than 2,000 kg/m^3 has the effect of thinning the sedimentary overburden, and modeling it as more dense has the effect of thickening the sedimentary overburden. The models shown, therefore, likely represent the generalized shape of the top of the basement rocks in the subsurface, but the amplitude could be more or less dramatic than depicted at a given location, owing to both uncertainty and unmodeled variability of the density of the alluvium (see fig. 10). Because it is difficult to characterize the density of a thick section of heterogeneous alluvium, it is likely that the uncertainty in the model cannot be reduced without significant modeling effort or additional independent constraints. In addition to the uncertainty in the modeled alluvial layer, there is uncertainty in the density value used to represent the basement rocks, which also are likely to be internally heterogeneous. It follows from the uncertainty of the rock and sediment densities that models should necessarily be simple, in this case modeling no more than two layers and using as few nodes as possible to define the shape of the subsurface units. The simple two-layer models capture the overall characteristics of the subsurface without overfitting the data.

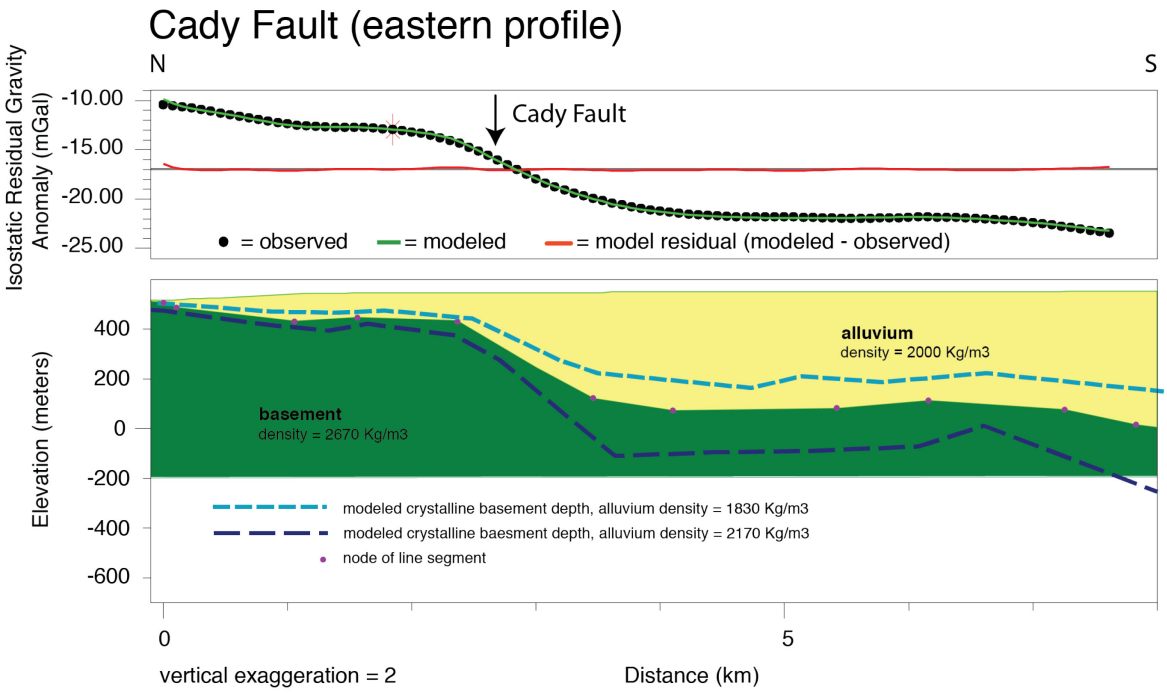

Figure 10. Modeled cross-section across the Cady Fault, Barstow, California, with dashed lines showing the effect of uncertainty in the density value used to model the alluvial sediments. Arrow indicates where east-striking cross-section line crosses perpendicular to this cross-section.

Three profiles (fig. 3), two across the Cady Fault and one across the Manix and Cave Mountain faults, were modeled by using interpolated data generated from the combined new and historical dataset because amplitude of the gravity anomalies along these profiles (10–15 mGal) was much greater than the estimated error in the gravity data (±0.1 mGal). Because the error in the isostatic gravity is small relative to the gravitational anomalies present in these profiles, such errors have little effect on the model produced.

Two profiles, across the Toomey Hills (the westernmost end of the Manix Fault) and Calico Fault (fig. 3), were modeled using only the newly collected gravity data, not the interpolated gravity dataset used above, because the amplitude of the gravity anomalies (~1 mGal) was not more than an order of magnitude greater than the estimated error in the data (±0.1 mGal). Because the error in the historical data is likely larger than the error in the newly collected data, and because ensuring the two datasets are on the exact same datum is not possible, only the newly collected data were used. This avoids potential anomalies caused by uncertainty in the value and bias of the historical data when compared with the newly collected data.

Both the historical gravity data and the newly collected gravity data were combined into one gravity dataset for the study area and were interpolated into a smooth surface of the isostatic residual-gravity anomaly (fig. 2). The interpolation algorithm used was the default algorithm available in the Oasis montaj software (Geosoft, Inc., 2006), and is based on the bicubic spline algorithms of Briggs (1974) and Swain (1976) (Geosoft, Inc., 2006). Points of maximum local slope (horizontal gradient) on the surface were calculated according to the method of Phillips and others (2007) (fig. 4), which when forming elongate strings of points, can indicate geologic structure in the subsurface (Blakely, 1995).

Results

The technological modifications to the survey workflow provided an effective way to collect, process, analyze, and interpret the data during the field session. The modified workflow was helpful because preliminary modeling was used to guide targeted data collection for the latter part of the survey. The workflow also necessitated regular downloading and processing of the data each evening. This requires time for processing and analyzing the data in the evenings, but also helps ensure that the data are reviewed and any problems that arise can be addressed immediately. Processing and analyzing the data each day also encourages one to make regular back-ups. Real-time streaming of satellite-map data to the iPad was also a significant benefit to navigation, and GIS and other iPad apps, such as Microsoft Excel, enabled navigational data and notes to be recorded easily.

The interpolated surface generated from the combined gravity dataset, and the resulting gradient points (fig. 4), indicate possible locations of subsurface structures. The gradients are generated by abrupt vertical to subvertical changes in density in the subsurface, as might occur when two disparate units are juxtaposed across a fault. The gradient points denote the location of an abrupt change in rock density in the subsurface caused by a vertical contact. Gradient points are, therefore, a good guide to locating larger structures, such as the Cady, Manix, or Cave Mountain faults, where surface expression is lacking. Gradient points also can be generated by artifacts in the data. For example, an isolated data point may, when gridded, produce a local maximum on the surface (several of these are visible in fig. 4), causing gradient points to encircle the data point. Gradient points that occur in highly curved strings are often artifacts caused by the tendency of the gridding algorithm to form smooth hummocks in regions of sparse data coverage. Whether gradients points are due to a surface artifact or a geologic feature is a matter of interpretation; mapped surface geology, structural interpretation, and modeled cross-sections were considered to make this determination. One way to enhance the interpretation of a string of gradient points as linear features is to display each point as a short line that is oriented in a direction perpendicular to the direction of maximum slope. In this way gradient points that are oriented in a line along a steep slope appear as a single linear feature (fig. 4).

The modeled cross-sections work in concert with the gradient points. This is because the modeled cross-sections have excellent resolution in the plane perpendicular to structure, but no resolution along strike. The gradient points highlight the strike of structural features, but the exact location and depth of the structures are poorly resolved.

The modeled cross-sections reveal topographic displacements in the basement rocks, likely representing offsets, across the Cady, Manix, and Cave Mountain faults (figs. 10–12). Maximum and minimum topographic offsets are shown for the cross-section across the Cady Fault in order to demonstrate the possible thicknesses of alluvium that range in density from 1,830 kg/m^3 to 2,170 kg/m^3. As shown, the amplitude changes, but the overall shape of the topographic surface of the dense basement remains the same. The location of possible fault offset does not change, but the magnitude of the vertical offset does.

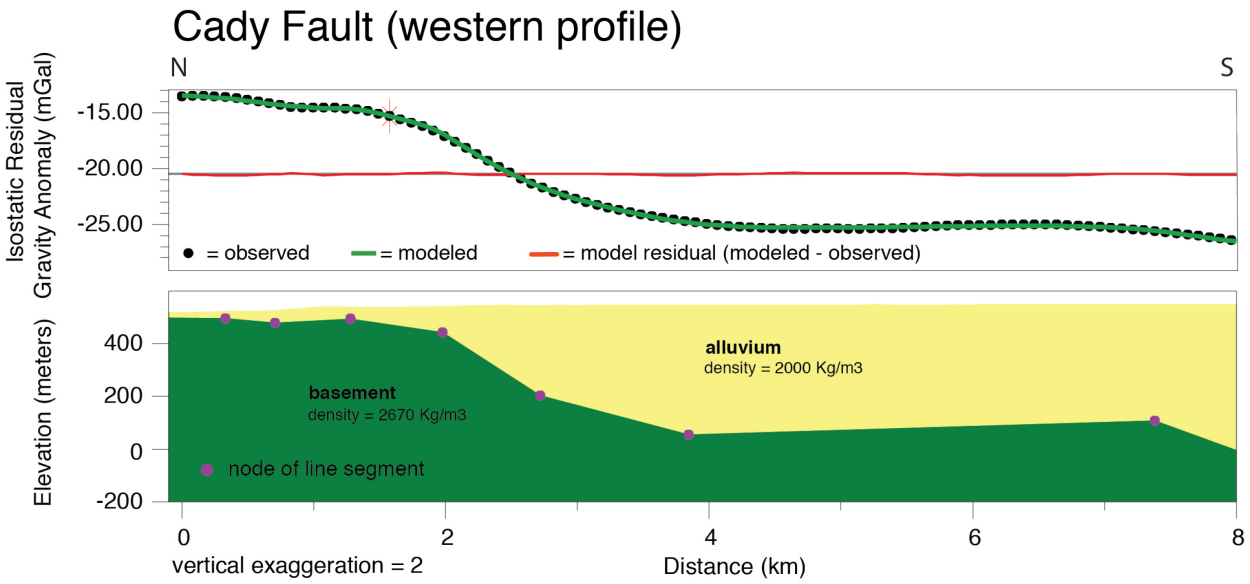

Figure 11. Modeled cross-section across the Cady Fault, Barstow, California. Model uncertainty is not shown, but is similar to that shown in figure 10.

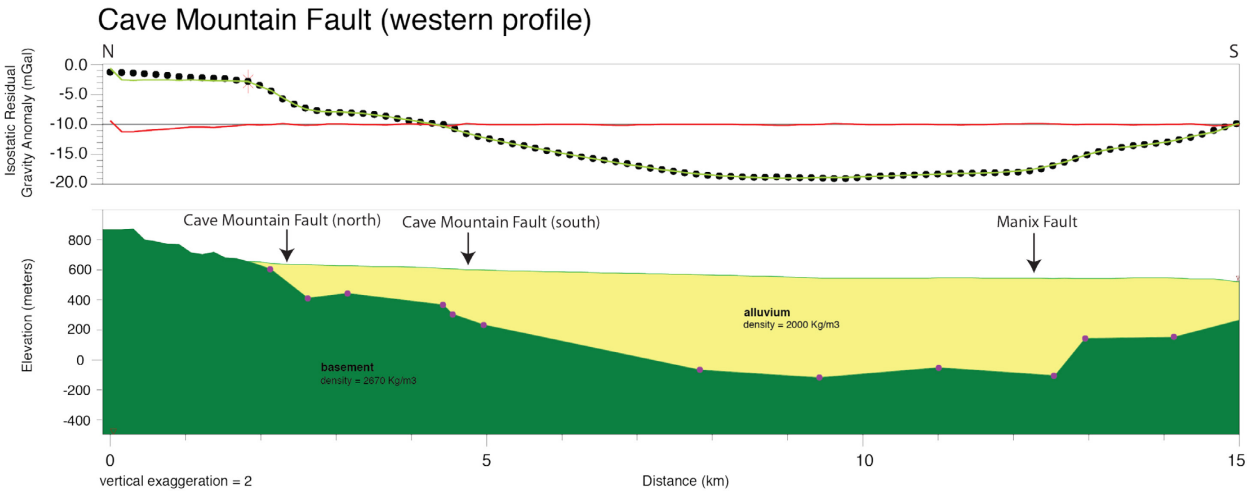

Figure 12. Modeled cross-section across the northern and southern strands of the Cave Mountain Fault, and across the Manix Fault, Barstow, California. Model uncertainty is not shown, but is similar to that shown in figure 10.

The effect of the uncertainty in density of the alluvial sediments can be contrasted with the effect of the 0.1 mGal combined measurement and data reduction uncertainty present in the isostatic residual gravity anomaly. The uncertainty in the gravity data is less than the thickness of the black dot symbol used to display the data in the Cady and Cave Mountain cross-section models (figs. 10–12). The observed and modeled change in the gravitational field along these cross-sections is on the order of several mGal, far greater than the uncertainty in the isostatic residual gravity anomaly. The uncertainty that has the greatest effect on these cross-section models is the uncertainty in the density of the rock and sediment in the subsurface.

Modeled cross-sections across the Toomey Hills are significantly affected by the uncertainty in the isostatic residual gravity data and, are therefore, are unable to resolve basement topography. Although a suggestion of structural offset can be modeled in the Toomey Hills profile (fig. 13), such an offset was not easily modeled in two profiles investigated approximately 800 and 1,200 meters to the east (profiles not shown in this report). Furthermore, the uncertainty in the isostatic gravity anomaly is approximately 50 percent of the variation in the anomaly (within 0.5 km of the surface trace of the Manix Fault in the Toomey Hills, the measured isostatic gravity anomaly is, at most, 0.4 mGal). To demonstrate the effect of this uncertainty, a second model (fig. 13, dashed lines) was generated, deliberately flattening topography along the basement as much as possible while remaining within the error envelope of the isostatic gravity anomaly data. A model almost devoid of topography along the basement is permissible given the measurement and processing error of the gravity data. If the uncertainty in the material density were to be added, so many configurations of basement topography would be possible that any individual model would yield little predictive power. Differences in gravity values along the profile are too small to be clearly attributable to changes in basement topography, given the uncertainty in the gravity data and the density values of the rocks and sediments.

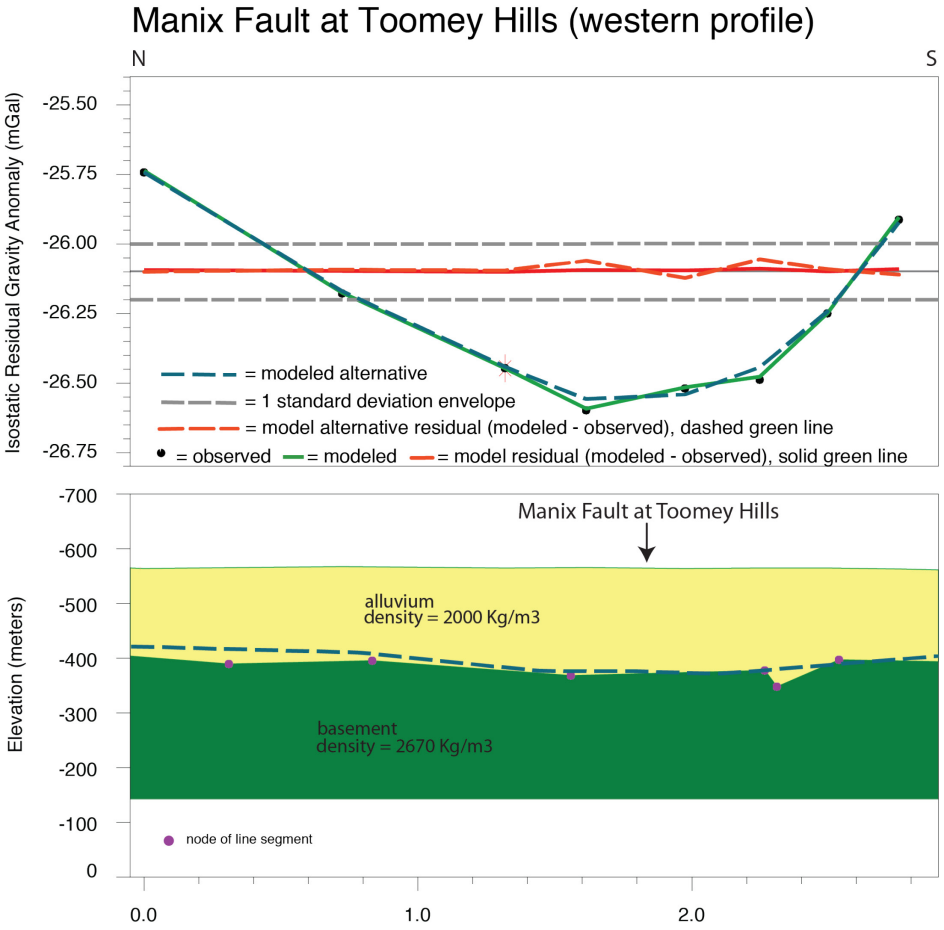

Figure 13. Modeled cross-section across the Manix Fault at the Toomey Hills, Barstow, California. Dashed lines show an alternative model that fits the data within the uncertainty envelope.

The modeled cross-section across the Calico Fault (fig. 14) has a high uncertainty associated with it, but not quite as high as the Toomey Hills cross-section. The uncertainty associated with the gravity anomaly profile is about 25 percent of the total anomaly amplitude. With the addition of the uncertainty in the density of materials, the variability in modeling is still significant. The coincidence of two local peaks in the isostatic gravity anomaly at almost the exact location of the Calico Fault and the Manix Fault at Toomey Hills, and the fact that the anomaly associated with the much larger Calico Fault has higher amplitude, suggests that these features are generating a gravity signal. However, the modeling is necessarily imprecise owing to the high uncertainty and lack of independent constraints, such as borehole data defining the depth of bedrock at one or more locations, or exposed bedrock at one end of the model.

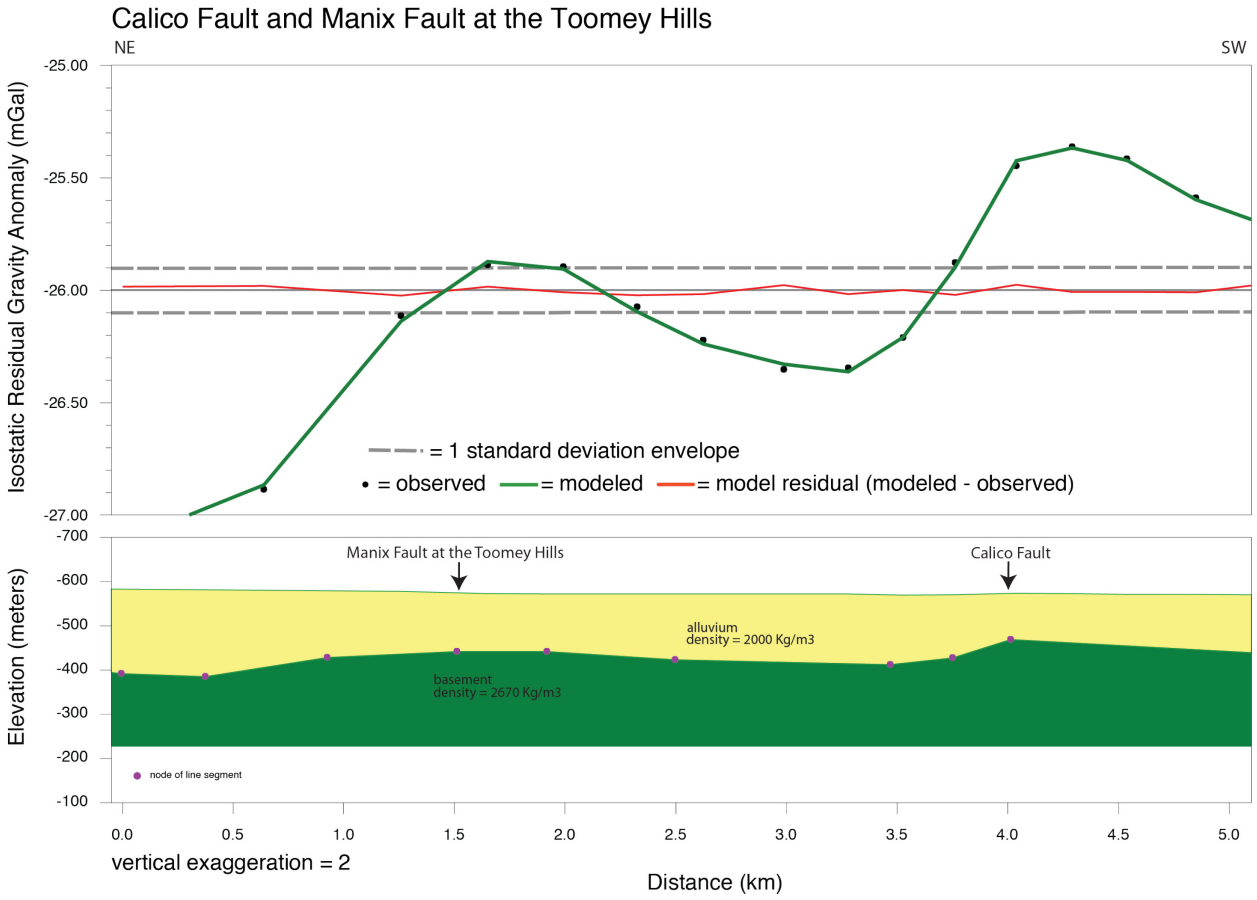

Figure 14. Modeled cross-section across the Calico and Manix Faults.

Discussion

The advent of real-time GPS data, spatial mapping software (geographic information system and geophysical software), a suite of imagery, geologic, elevation, and other data sets, all laptop-enabled, now gives researchers the option to focus on interpreting results, testing, and modifying hypotheses during a single field session. This enhancement of data-collection methods portends an integrated approach to geologic fieldwork, where geologic and geophysical data could be collected concurrently, and the resulting geologic hypotheses tested and revised during a single field session.

During the 2011 survey, preliminary modeling of cross-sections across the Cady Fault, and the Manix Fault at Toomey Hills, lead to a decision to modify the survey and collect additional data across these structures, successfully demonstrating that current technology can be used to accelerate the timeframe for processing data and optimizing data collection. The resulting cross-sectional models clearly show basement offset along the Cady Fault. The second (western) profile and resulting model show that the Cady Fault begins to curve and trends in a more northerly direction, apparently merging with the Manix Fault. Vertical offset across the Cady Fault is on the order of 300 m, or between 200 and 500 m when the uncertainty in the density of the alluvium is taken into account. The amount of vertical offset appears consistent from one profile to the other. In the case of the Manix Fault at Toomey Hills, the preliminary suggestion of a subsurface structure was not repeatable across subsequent profiles. Additional modeling, taking into consideration the uncertainty in the data, showed that the precision of the available data was not high enough to resolve the geologic structure of interest. Although this is a "negative result" lack of visible structure indicates that the mapped Manix Fault at Toomey Hills does not cause appreciable vertical offset of basement rocks and could be a small, local feature in this region. Both investigations answered follow-up questions from data collected during the initial phase of the survey. Without augmenting the survey workflow to take advantage of technological improvements, these questions would have remained unanswered pending new data collected in a future field season.

Two subsurface structures are apparent along the Cave Mountain profile (fig. 12). The cross-sectional model shows a 200 m apparent down-drop on the northern strand of the Cave Mountain Fault, along the southern front of the Alvord Mountains, and a 200 m apparent down-dropped section across the Manix Fault. Because both the Cave Mountain and Manix Faults are left-lateral strike-slip faults, the apparent down-drop could be the result of oblique-slip motion, or of the juxtaposition of different rocks and sediments due to lateral motion. The southern strand of the Cave Mountain Fault appears to generate a low, gradual slope in the subsurface.

Modeling of the Calico Fault suggests two minor subsurface structures may exist related to the low-amplitude isostatic residual gravity anomalies that are spatially coincident with the Calico Fault and the Manix Fault at Toomey Hills. Although uncertainty is high in these models, the anomalies are measurable and spatially coincident with the traces of the faults. The degree of geologic structure that is present in the subsurface is, however, more uncertain, and a range of basement configurations could be fit to the gravity anomaly data within the error tolerance.

The initial depth of the basement surface for both the Calico and Toomey Hills profiles was set arbitrarily at 400 m. This yielded modeled anomalies of a large enough wavelength that they smoothly fit observations. However, the mean depth of the surface could be modeled as shallower or deeper. Further investigation should include any independent estimates of depth to basement (drill-hole data, data projected from outcrop), although the variability in the density of the materials could still be a significant source of uncertainty for modeling the shape of the basement surface.

The gradient points (fig. 4) that highlight the local slope on the interpolated isostatic residual gravity surface are clearly artifacts in many places where sparse data generates steep local slopes around data points. However, where data are denser, the gradient points are generally near mapped faults, indicating a change in the density of material in the subsurface. For example, along the Cave Mountain transect, gradient points occur near or on strike with both strands of the Cave Mountain Fault and the Manix Fault. The same is true of the Cady Fault profiles. In these cases the gradient points can be used to trace the probable location of the faults

in the subsurface, provided the density of data points remains high. For example, the Cady Fault could be mapped in the subsurface along the gradient points that pass through both the east and west profiles and continue at least 3 km to the west.

Conclusions

The technological modifications to the survey workflow promises an increase in the efficiency of gravity surveying because the focus shifts away from data collection and toward the iterative process of data collection, analysis, modeling, hypothesis generation, and further data collection to test the hypotheses. The modifications also pave the way for integrated, cross-disciplinary fieldwork, where geologic and geophysical mapping techniques, for example, can be simultaneously brought to bear on a scientific problem during a single field session.

Increase in the regional coverage of gravity data has constrained the negative gravity anomaly over the Yermo Hills and the positive gravity anomaly northeast of the Cady Mountains. The Yermo Hills are a region of sediment accumulation in a local structural basin, whereas northeast of the Cady Mountains, dense bedrock likely lies just below the surface.

The Cady, Cave Mountain, and Manix faults clearly offset rock units in the subsurface. Modeled vertical offsets are approximately 300 m, although uncertainty in model parameters allows for a range of at least 200–500 m. The Calico Fault appears to vertically offset subsurface rock units by somewhat less than 100 meters, and the western trend of the Manix Fault at Toomey Hills may also exhibit a slight subsurface vertical offset, although the uncertainty for this model is high. The eastern trend of the Manix Fault at Toomey Hills does not produce a large enough gravitational anomaly to be modeled with certainty.

References Cited

Blakely, R.J., 1995, Potential theory in gravity and magnetic applications: New York, Cambridge University Press, 441 p.

Biehler, S., Tang, R.W., Ponce, D.A., and Oliver, H.W.,1988, Bouguer Gravity Map Of The San Bernardino Quadrangle, California, 1:250,000: California Division Of Mines And Geology Regional Geologic Map Series, map no. 3B.

Briggs, I., 1974, Machine contouring using minimum curvature: Geophysics, v. 39, no. 1, p. 39–48.

Dobrin, M.B., and Savit, C.H., 1988, Introduction to geophysical prospecting (4th ed.): McGraw-Hill, 867 p.

Dokka, R.K., and Travis, C.J., 1990, Late Cenozoic strike-slip faulting in the Mojave Desert, California: Tectonics, v. 9, no. 2, p. 311–340.

Garfunkel, Z., 1974, Model for the Late Cenozoic tectonic history of the Mojave Desert, California, and for its relation to adjacent regions: Geological Society of America Bulletin, v. 85, no. 12, p. 1931–1944.

Geosoft, Inc., 2006, Montaj gravity and terrain correction: Gravity Data Processing Extension for Oasis montaj v6.3 Tutorial and User Guide, accessed May 9, 2013, at: http://www.geosoft.com/.

Gesch, D.B., 2007, The National Elevation Dataset, *in* Maune, D., ed., Digital elevation model technologies and applications—The DEM users manual, (2d. ed.): Bethesda, Md., American Society for Photogrammetry and Remote Sensing, p. 99–118, accessed June 2011 at http://nationalmap.gov/.

Gesch, D., Oimoen, M., Greenlee, S., Nelson, C., Steuck, M., and Tyler, D., 2002, The National Elevation Dataset: Photogrammetric Engineering and Remote Sensing, v. 68, no. 1, p. 5–11.
Kane, M.F., 1962, A comprehensive system of terrain corrections using a digital computer: Geophysics, v. 27, no. 4, p. 455–462.
Karki, P., Kivioja, L., and Heiskanen, W.A., 1961, Topographic isostatic reduction maps for the world for the Hayford Zones 18-1, Airy-Heiskanen System, T=30 km: Publication of the Isostatic Institute of the International Association of Geodesy, no. 35, 5 p., 20 pl.
La Fehr, T.R., 1991, An exact solution for the gravity curvature (Bullard B) correction: Geophysics, v. 56, no. 8, p. 1179–1184.
Langenheim, V.E., Biehler, S., Negrini, R., Mickus, K., Miller, D.M., and Miller, R.J., 2009, Gravity and magnetic investigations of the Mojave National Preserve and adjacent areas, California and Nevada: U.S. Geological Survey Open-File Report 2009–1117, 25 p.
Li, X., and Gotze, H., 2001, Tutorial ellipsoid, geoid, gravity, geodesy, and geophysics: Geophysics, v. 66, no. 6, p. 1,660–1,668.
Lowrie, W., 1997, Fundamentals of geophysics: Cambridge, UK, Cambridge University Press, 354 p.
Miller, D.M., Dudash, S.L., Green, H.L., Lidke, D.J., Amoroso, L., Phelps, G.A., and Schmidt, K.M., 2007, A new Quaternary view of northern Mojave Desert tectonics suggests changing fault patterns during the late Pleistocene, *in* Miller, D.M. and Valin, Z.C., eds., Geomorphology and tectonics at the intersection of Silurian and Death valleys, southern California: U.S. Geological Survey Open-File Report 2007–1424, p. 157–171.
Morelli, Carlo, ed., 1974, The International Gravity Standardization Net 1971: International Association of Geodesy Special Publication no. 4, 194 p.
Nagy, D. 1966. The gravitational attraction of a right rectangular prism: Geophysics, v. 31, no 2., p. 362–371.
National Geodetic Survey, 2003, Vertcon—Version 2.1, accessed June 2011 at http://www.ngs.noaa.gov/PC_PROD/VERTCON/.
Nettleton, L.L., 1971, Elementary gravity and magnetics for geologists and seismologists: Tulsa, Okla., Society of Exploration Geophysicists Monograph Series, no. 1, 121 p.
Pan-American Center for Earth and Environmental Studies, 2010, Gravity database, accessed January 8, 2010, at http://irpsvgis00.utep.edu/repositorywebsite.
Phelps, G.A., Bedford, D.R., Lidke, D.J., Miller, D.M., and Schmidt, K.M., 2011, Preliminary Quaternary geologic map and database of the Newberry Springs 30' x 60' quadrangle, California: U.S. Geological Survey Open-File Report 2011–1044, 101 p.
Phelps, G.A., Langenheim, V.E., and Jachens, R.C., 1999, Thickness of Cenozoic deposits of Yucca Flat inferred from gravity data, Nevada Test Site, Nevada: U.S. Geological Survey Open-File Report 99–310, 33 p.
Phillips, J.D., Hansen, R.O., and Blakely, R.J., 2007, The use of curvature in potential field interpretation: Exploration Geophysics, v. 38, p. 111–119.
Roberts, C.W., and Jachens, R.C., 1986, High-precision gravity stations for monitoring vertical crustal motion in southern California: U.S. Geological Survey Open-File Report 86-44, 76 p.
Ron, H., Beroza, G., and Nur, A., 2001, Simple model explains complex faulting: Eos, Transactions, American Geophysical Union, v. 82, no. 10, p. 125, 128–129.
Simpson, R.W., Jachens, R.C., Blakely, R.J., and Saltus, R.W., 1986, A new isostatic residual gravity map of the conterminous United States with discussion on the significance of isostatic residual anomalies: Journal of Geophysical Research, v. 19, no. B8, p. 8348–8372.

Snyder, D.B., Roberts, C.W., Saltus, R.W., and Sikora, R.F., 1982, A magnetic tape containing the principal facts of 64,026 gravity stations in the state of California: available from National Technical Information Service, U.S. Department of Commerce, Springfield, Va., 22152,PB 82-168287 [description of magnetic tape, PB 82-168279], magnetic tape, 34 p.

Swain, C.J., 1976, A fortran IV program for interpolating irregularly spaced data using the difference equations for minimum curvature: Computers and Geosciences, v. 1, p. 231–240.

Swick, C.A., 1942, Pendulum gravity measurements and isostatic reductions: U.S. Coast and Geodetic Survey Special Publication 232, 82 p.

Telford, W.M., Geldart, L.P., and Sheriff, R.E., 1990, Applied geophysics (2d ed.): Cambridge, UK, Cambridge University Press, 770 p.

Trimble Navigation Limited, 2005, H-Star technology explained—Trimble Navigation Limited white paper: accessed September 1, 2011, from www.esri.com/partners/hardware/h-star_explained.pdf.